HIGH RESOLUTION X-RAY DIFFRACTION AND SCANNING ELECTRON MICROSCOPY INVESTIGATIONS OF THE SAW PROPAGATION IN PERFECT $La_3Ga_5SiO_{14}$ CRYSTALS

D.V. Roshchupkin[1*], D.V. Irzhak[1], O.A. Buzanov[2], S.A. Sakharov[2], R. Tucoulou[3]

[1]Institute of Microelectronics Technology, Russian Academy of Sciences, 142432 Chernogolovka, Moscow District, Russia
[*]e-mail: rochtch@ipmt-hpm.ac.ru
[2]FOMOS Technology Co., 105023 Buzheninova Str. 16, Moscow, Russia
[3]ESRF, BP 220, F-38043 Grenoble Cedex 09, France

ABSTRACT

This paper reports a scanning electron microscopy visualization of surface acoustic waves propagation in *Z*-cut of a $La_3Ga_5SiO_{14}$ crystal. Also we present an experimental study by X-ray Bragg diffraction of a Rayleigh surface acoustic waves propagating in (220)-cut of a $La_3Ga_5SiO_{14}$ crystal. Many parameters such as acoustic amplitude, the reflection number, and the X-ray energy were varied, thereby providing an extensive view of the acousto-optic interaction in the crystal. It is shown that the X-ray diffraction spectra depend strongly on the ratio of the X-ray and acoustic penetration depth.

Keywords: surface acoustic waves; scanning electron microscopy; x-ray diffraction.

1. INTRODUCTION

The development of acousto-electronic devices based on surface acoustic waves (SAW) has been very active in the fields of filters, oscillators, real-time processing systems, and convolvers, etc., which are widely used in new communication systems (mobile phones, radio systems, TV, GPS). This development is accompanied by an increasing need for precise characterization of the acoustic fields in these devices. Here, we present experimental results demonstrating the new possibility of scanning electron microscopy method (SEM) and X-ray diffraction for the qualitative and quantitative analysis of the SAW propagation in perfect $La_3Ga_5SiO_{14}$ crystals (LGS).

LGS crystals were grown along axis Z using the Chzochralski technique by "FOMOS Technology" Company.

2. SEM IMAGING OF THE SAW

The SEM method in the mode of secondary electron recording was used as an experimental technique for visualization of the SAW in LGS since only low energy secondary electrons with energy ~1-3 eV are sensitive to the electric field which accompanies the propagation of the traveling SAW in piezoelectric materials. The SAW was rendered visible in a JSM-840 scanning electron microscope with an accelerating voltage E_0=1 kV and a probe current I_0=1 nA. The use of higher accelerating voltage is not possible, because the piezoelectric substrate would be highly charged and thus bring about a distortion of the image because of deflection of the electron probe and the change in the secondary electron emission from the surface. The principle of the traveling SAW imaging is based on the high-frequency modulation of the low energy secondary electrons by a stationary electrostatic interference field formed above the crystal surface by the interaction between the varying electric field of the SAW and the component, normal to the surface, of the electromagnetic radiation field of the interdigital transducer (IDT). The electromagnetic and acoustic waves are mutually coherent, since they are excited by the same source (IDT) and with the same frequency. Since the wavelength of the electromagnetic wave is large than the SAW wavelength, the period of the stationary interference field is equal to the SAW wavelength. Under these conditions, the low energy secondary electrons are modulated by the stationary electrostatic interference field (Refs 1-2).

The *Z*-cut of a LGS was used for the SAW excitation. For excitation of the SAW an IDT with a finger width of 7-μm and 28-μm SAW wavelength was formed on the crystal surface so that SAW propagates in the direction of *X*+39˚. The SAW velocity in this direction is *V*=2372 m/s. Fig. 1 shows the SEM photomicrographs of the propagation of the traveling SAW. Figure 1(a) is a SEM micrograph of the radiation pattern of Rayleigh SAW excited by an IDT at the resonance frequency *f*=84.73 MHz and at an amplitude of the input signal on the IDT *U*=4 V. It is seen from the SEM images (Fig. 1(a) and 1(b)) that the power–flow angle (PFA) equals φ=-13˚, i.e., the angle between the direction of the power-flow vector (PFV) and the direction of the SAW propagation. Fig. 2(c) shows the SEM image of the pseudo SAW (PSAW) excited by an IDT at the resonance frequency *f*=96.87 MHz. The PSAW velocity is *V*=2712 m/s. The PFA for the PSAW equals φ=+23˚. It is seen from Fig. 1 that the SAW and PSAW have the different directions of the PFV.

Thus we have shown, that the scanning electron microscopy method can be used directly for characterization of the SAW propagation in the LGS crystals.

3. X-RAY DIFFRACTION FROM LGS CRYSTAL MODULATED BY SAW

X-ray diffraction has been used to study the characteristics of SAW fields propagating inside crystals. The main result of X-ray interaction with SAW is the rise of diffraction satellites in the reflectivity measurements. Some experiments have already been carried out on Bragg diffraction on SAW in Si (Ref. 3) and $LiNbO_3$ crystals (Ref. 4).

3.1 The SAW device

Acoustic waves of Rayleigh type were produced by photolithographically deposited IDT upon perfect LGS crystal. We have used (220)-cut of LGS crystal. SAW wavelength Λ=12 μm was excited at resonance frequency *f*=192.5 MHz. Rayleigh waves are elliptically polarized, but in specular Bragg geometry, longitudinal displacements do not affect X-ray diffraction. Therefore a Rayleigh wave can be approximated as a sinusoidal modulation normal to the diffraction atomic plane. The propagation of a SAW induces deformation in the bulk far below the surface. Calculation have shown that the SAW penetration in (220)-cut of LGS crystal should extend to a depth of the order of a SAW wavelength (Fig. 2), i.e. ~12 μm in this case.

Since the SAW velocity (*V*=2310 m/s) is much lower than the speed of the X-rays, the acoustic deformation can be considered as quasistatic and characterized by its wavelength and amplitude. Assuming an exponential damping of the SAW amplitude in the bulk, the vertical displacements

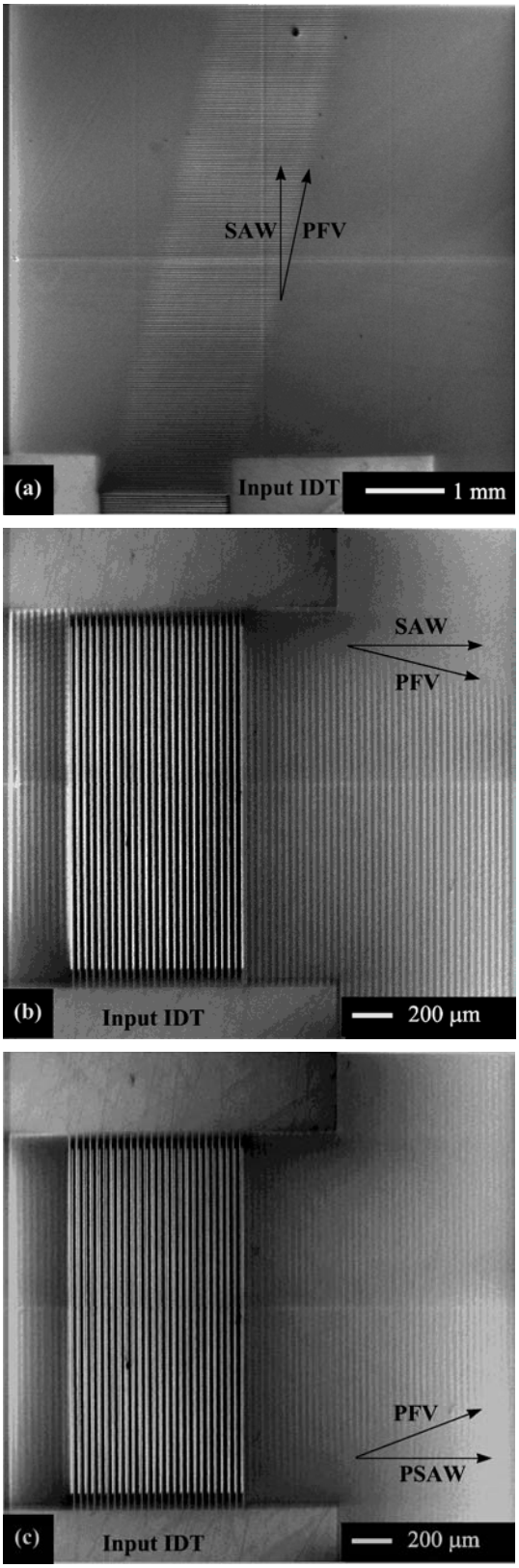

FIG. 1. SEM photomicrographs of the traveling SAW: (a), (b) Rayleigh SAW, f=84.73 MHz; (c) PSAW, f=96.87 MHz.

of atoms of coordinates (x,y,z) can be written approximated as

$$h=h_0\exp(-\mu_{SAW}z)\exp(iKx), \quad (1)$$

with μ_{SAW}^{-1} the SAW penetration depth, K the SAW wave vector, z the crystal depth. The SAW amplitude h_0 could be

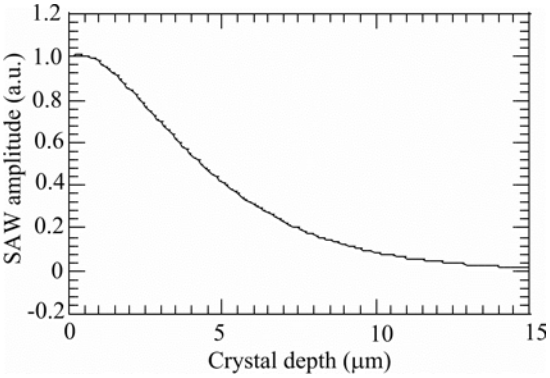

FIG. 2. Calculated SAW amplitude (h) vs crystal depth.

varied from 0 to a few angstroms by varying of the voltage supplied to the IDT.

3.2 The X-ray/SAW interaction

X-ray diffraction on the modulated atomic planes leads to the formation of satellites on both sides of the Bragg peak along which constructive interference induced by the SAW occur. In the symmetric Bragg case, these angular direction can be deduced from the grating equation:

$$\sin\theta_m=m\lambda_{SAW}/2d+\sin\theta_B, \quad (2)$$

where θ_B the incident Bragg angle, m the diffraction order number, and θ_m the exit angle of the mth order satellite.

In the case of a rocking curve measurement with the detector placed at twice the Bragg angle, $\theta_{mRC}=\theta_B+\delta\theta_{mRC}$ and $\theta_m=2\theta_B-\theta_{mRC}$ where θ_{mRC} is the angle of the mth order satellite given by the rocking curve. Using equation (2) and supposing that $\delta\theta_{mRC}$ can be written as

$$\delta\theta_{mRC}=m\lambda/2d\cos\theta_B=m\Delta\theta \quad (3)$$

where d is the interplanar spacing.

3.3 Experimental setup

X-ray diffraction experiment was carried out at the optics beamline (BM05) of the ESRF. The energy of X-ray radiation was selected by a double Si(111) monochromator, diffracting in the vertical plane.

Primary and secondary slits having horizontal and vertical gaps of 1*1 mm and 0.1*0.1 mm, respectively, were placed as shown in Fig. 3. A double-axis diffractometer diffracting in the horizontal plane was used to obtain sufficient angular resolution (~0.1 arc.sec.) to separate the successive diffraction satellites clearly. Another monochromator Si(333) was insert before the sample to obtain a highly monochromated X-ray beam ($\Delta\lambda/\lambda\approx10^{-6}$). A Cyberstar NaI scintillation counter was used for the detection.

3.4 Experimental results

The diffraction spectra of the (220)-cut of a modulated LGS crystal were measured for different reflections ((110), (220) and (330)) at different X-ray energy (E=11, 17, 25 keV).

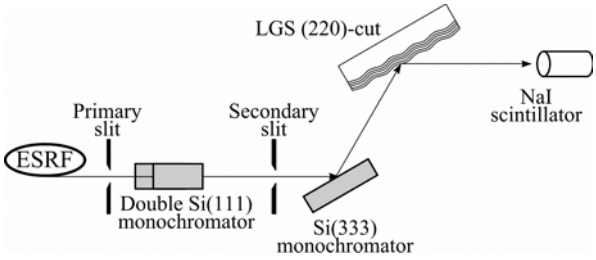

FIG. 3. Experimental setup.

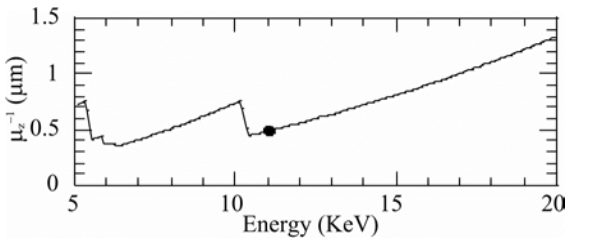

FIG. 4. X-ray penetration depth in a LGS crystal for (110) reflection vs energy. Black circle shows the energy E=11 keV.

The most import result was obtained for (110) reflection at X-ray energy E=11 keV because of very small X-ray penetration depth. The d spacing of the (110) reflection for LGS crystal is d=4.087 Å. Based on kinematic diffraction theory, the profile of the X-ray penetration depth due to absorption in LGS as a function of energy $\mu_z^{-1}(E)= \sin(\Theta_B(E))/2\mu_L(E)$ is plotted in Fig. 4 (μ_L is the linear absorption coefficient; Θ_B is the incident Bragg angle). The presence of the K-edge of Ga at 10.47 keV introduces a sharp variation of μ_z^{-1} in this region. At E=11 keV the X-ray penetration depth is only μ_z^{-1}=0.48 μm, which is more smaller than the SAW penetration depth. This case, when X-ray penetration depth is more smaller then the SAW penetration depth (E=11 keV), corresponds to the conditions of kinematic diffraction ($\mu_z^{-1}/\mu_{SAW}^{-1}<1$).

Fig. 5 shows several rocking curves of the LGS (110) reflection from a (220)-cut crystal recorded for various amplitudes of the input signal on an IDT (U) for a SAW wavelength Λ=12 μm and at fixed X-ray energy of 11 keV. The incident Bragg angle is Θ_B=7.92˚. The full width at half-maximum (FWHM) of the Bragg peak without SAW excitation is 3.2 arc.sec. (Fig. 5(a)).

It can be seen that the number of visible diffraction satellites increases with the acoustic amplitude. The angular deviation $\delta\Theta_{mRC}$ between adjacent diffraction satellites is 6.8 arc.sec. which corresponds well to the calculated value from equation (3) 7.0 arc.sec.

At the amplitude of the input signal on an IDT U=8.5 V it can be seen that the intensity of the m=0 diffraction satellite practically equals to zero (Fig. 5(b)). It is due with the fact that the phase shift of X-ray radiation diffracted from the SAW minimum and maximum into the m=0 order equals to π. The intensity of the m=+1(-1) diffraction satellites reaches a minimum at the amplitude of the input signal on an IDT U=14 V (Fig. 5(c)).

Fig. 6 shows the variation of several successive diffraction satellites (m=0, 1, 2) as a function of the amplitude of the input signal supplied to the IDT at the X-ray energy of E=11 keV. A particular satellite can be observed only if the amplitude of the input signal is above the threshold value, which increases with the diffraction order. Once the amplitude of the input signal exceeds this threshold, the satellite intensity increases rapidly, reaches a maximum and then decreases with smooth oscillations down to an asymptotic value.

Using a simple kinematic model developed in Ref. 4 it is possible to calculate the intensity of the diffraction satellites. The mth order satellite intensity is proportional to

$$I_m \propto \left| \int_0^\infty e^{-\mu_z z} J_m\left(h_0 q_z e^{-\mu_{SAW} z}\right) dz \right|^2, \qquad (4)$$

where J_m the Bessel function; q_z the component of the diffraction vector $Q(q_x, 0, q_z)$, normal to the atomic plane; z the crystal depth. Therefore each satellite intensity can be calculated from the acoustic amplitude at the crystal surface

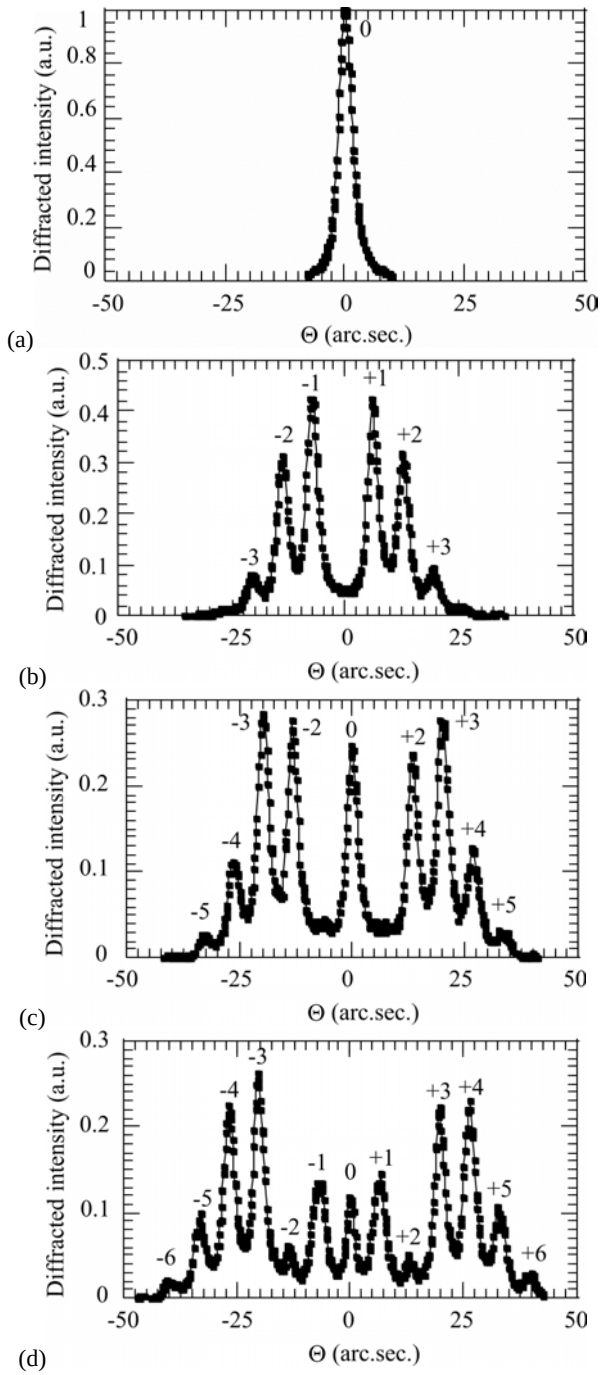

FIG. 5. Rocking curves measured for different amplitudes of the input signal supplied to the IDT: (a) U=0 V, (b) U=8.5 V, (c) U=14 V, (d) U=18 V. E=11 keV; Λ=12 μm; (110) reflection.

and from the acoustic and X-ray penetration depth.

The solid lines in Fig. 6 shows the calculated data of the diffraction satellite intensities as a function of the SAW amplitude at the crystal surface. These calculated results are in a good agreement with experimental one. Thus, using experimental diffraction spectra and simple kinematic model it is possible to determine the SAW amplitude at the crystal surface and acoustic penetration depth.

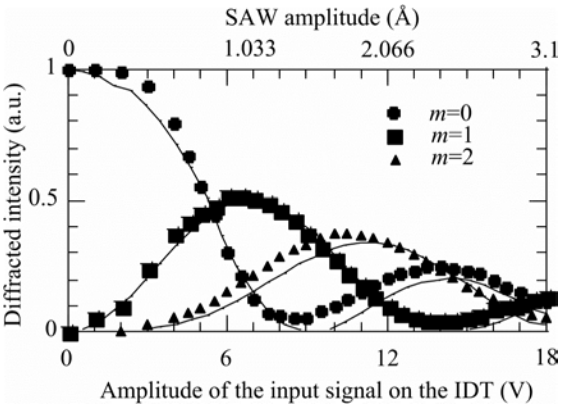

FIG. 6. Intensities of the diffraction satellites (m=0, 1, 2) vs amplitude of the input signal supplied to the IDT U (or vs calculated SAW amplitude h_0). Black circles, squares, triangles: experimental data; solid lines: calculated data. *E*Å. . Bas ed Å. o nk ei. . mt cafra˚ Tul w

4. CONCLUSION

It has been shown that the SEM and high-resolution X-ray diffraction can be used directly for qualitative and quantitative analysis of the SAW propagation in LGS crystal.

The SEM is useful for visualization of the excitation of acoustic radiation field on the crystal surface. It is possible to use this method for determination of the direction of the PFV and for measurement of the PFA.

High-resolution X-ray diffraction technique can be used for determination of amplitude and SAW wavelength, acoustic penetration depth.

ACKNOWLEDGEMENTS

This work has been supported by a joint program between the CNRS and IMT RAS. Two of us (D.V. Roshchupkin and D.V. Irzhak) are indebted to the Russian Foundation for Basic Research (Contract No. 00-02-16045).

REFERENCES

1. D. V. Roshchupkin, T. Fournier, M. Brunel, O. A. Plotitsyna, N. G. Sorokin, *Appl. Phys. Lett.*, vol. 60, pp. 2330-2331, 1992.
2. D. V. Roshchupkin, M. Brunel, *IEEE Trans. Ultrason. Ferroelectrics Freq. Cont.*, vol. 41, pp. 512-517, 1994.
3. R. Tucoulou, R. Pascal, M. Brunel, O. Mathon, D. V. Roshchupkin, I.A. Schelokov, E. Cattan, D. Remiens, *J. Appl. Cryst*., vol. 33, pp. 1019-1022, 2000.
4. R. Tucoulou, F. de Bergevin, O. Mathon, D. Roshchupkin, *Phys. Rev. B*, vol. 64, pp. 134108(9), 2001.